Comparative Analysis between PI & Backstepping Control Strategies of DFIG Driven by Wind Turbine

Mohamed Nadour*, Ahmed Essadki*, Tamou Nasser**

* Laboratory of Research in Electrical Engineering, Higher Normal School of Technical Education (ENSET), Mohammed V University, 10100, Rabat, Morocco

** Laboratory of Research in Electrical Engineering, Higher National School of Computer Science and Systems Analysis (ENSIAS), Mohammed V University, BP 713, Rabat, Morocco

(mohamed.nadour@um5s.net.ma, ahmed.essadki1@gmail.com, tnasser@ensias.ma)

‡ Corresponding Author; Mohamed Nadour, Morocco, Tel: +212 666 508 241,
, mohamed.nadour@um5s.net.ma

Received: 14.02.2017 Accepted: 08.04.2017

Abstract- This paper presents the modelling and control designs of Double-Fed Induction Generator (DFIG) integrated into a wind energy conversion system (WECS). The aim is to design and compare two distinct strategies of controlling independently the active and the reactive power generated by a DFIG, in order to conclude on their performances. In first place, a modelling of wind turbine and DFIG is presented. Then, the PI controller, the Backstepping approach and a maximum power point tracking (MPPT) strategy used to extract the maximum of power during the conversion are developed. Simulations results show significantly improved performances of the proposed backstepping approach over the Proportional-Integral controller, in terms of dynamic response, disturbance rejection, and robustness against parametric variations. The systems performances were tested and compared using *Matlab/Simulink* Software.

Keywords Wind energy conversion system, DFIG, PI, Backstepping, Maximum power point tracking, MPPT.

1. Introduction

In addition to other renewable energy sources, the wind energy is proving to be one of the preferred choices to produce electricity. Unlike fossil fuels, wind energy is clean, pollution-free from greenhouse gases emissions (CO_2) and inexhaustible. However, it is not powerful enough to replace the existing sources, this fact have attracted a lot of interests on the methods of exploitation and development of the wind energy conversion systems (WECS).

Over the years, several technologies have been proposed. In this paper, we focus on the grid connected, variable speed wind turbines equipped with double-fed induction generator (DFIG). Which is a wound rotor induction generator, where the stator windings are directly connected to the grid and the rotor winding are connected through back-to-back converter consists of two converters. i.e., rotor side and grid side converter, separated with a dc-link capacitor placed as energy storage, in order to keep the voltage variations small to the inverter [2,8]. DFIG is the most popular system among all WECS technologies, it due to its high-energy efficiency, less mechanical complexity, separately controllable active and reactive power, and a smaller power converter compared the same class of other generators (reduced losses and costs), about one third of the rated power for a variable speed generator operating at ± 30% of synchronous speed [14].

Over the past few decades, the classical control strategies that are normally based on linear PI controller presents suitable performances in many control applications. However, these techniques suffer many limitations, such as machine parameters variations. Therefore, various studies and new strategies of control have been invading the electrical engineering laboratories, in attempt to achieve high performances. During the pasts few years, there has been a massive amount of activity on a new special control schemes known as "Backstepping algorithms". With these control approaches, the feedback control laws that can ensure at the same time a good tracking response and stability of the overall system can be easily constructed. In this paper, it has been shown that replacing the PI controller by a backstepping control algorithm can significantly improve the tracking response and give excellent performances.

The paper is organized as follows. Section II presents a description and a detailed aerodynamic modelling of the variable speed wind turbine, the mechanical transmission system and the DFIG. Section III deals with both PI and backstepping control design, and a Maximum power point tracking "MPPT" strategy using backstepping controller to extract the maximum power from the wind velocity. Section IV simulation results performed by means of Matlab/Simulink software are presented and discussed, and then we finish by a conclusion.

2. Modelling of the Wind-Energy Conversion System

The wind-energy conversion system consists of the wind turbine, gearbox and DFIG **Fig.1**. The turbine captures the kinetic energy of the wind and converts it to a torque that rotates the rotor blades. Thereafter, the DFIG converts the mechanical power into an electrical power.

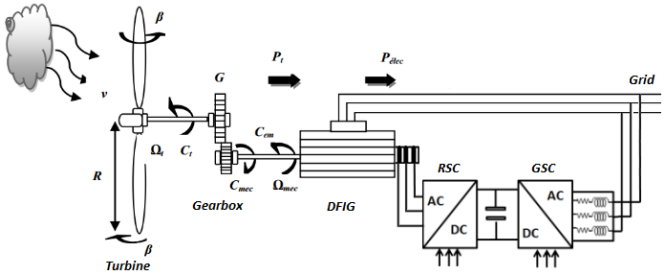

Fig. 1: Wind-energy conversion system

2.1. Modelling of wind turbine

The wind power that pass through a surface S is defined as follow (ρ is the density of air) [14]:

$$P_v = \frac{\rho S V_1^3}{2} \tag{1}$$

The aerodynamic power captured by the rotor is given by:

$$P_t = C_p(\lambda,\beta)P_v = C_p(\lambda,\beta)\frac{\rho S V_1^3}{2} \tag{2}$$

The power coefficient Cp represents the aerodynamic efficiency of the wind turbine. It depends on the blades orientation angle β and the tip speed ratio:

$$\lambda = \frac{R.\Omega_t}{V_a} \tag{3}$$

The expression of this power coefficient has been approached for this type of turbine, by the following equation [6]:

$$C_p(\lambda,\beta) = C_1\left(C_2\left(\frac{1}{\lambda+0.08\beta} - \frac{0.0035}{\beta^2+1}\right) - C_3\beta - C_4\right)$$
$$.\exp\left(-C_5\left(\frac{0.0035}{\lambda+0.08\beta).(\beta^2+1)} + C_6\lambda\right)\right) \tag{4}$$

C1=0.5109; C2=116; C3=0.4; C4=5; C5=21; C6=0.0068.

Fig.2 shows the power coefficient Cp curves for multiple values of β. These curves are characterized by an optimum point which is the point corresponding to maximum power coefficient, e.g. for β=0 (C_{pmax}=0.48; λ_{opt}=8.15).

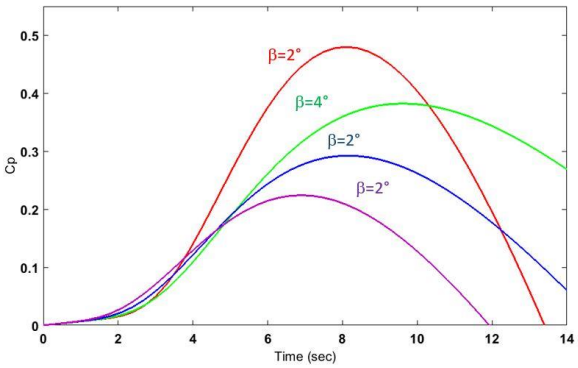

Fig. 2 : Power coefficient Cp

Expression of the aerodynamic torque is given by:

$$C_t = \frac{P_t}{\Omega_t} = C_p(\lambda,\beta)\frac{\rho S V_1^3}{2\Omega_t} \tag{5}$$

The gearbox is used as a connection, to adapt the speed of the turbine to that of the generator. The friction, elasticity and energy losses in the gearbox are neglected so:

$$\Omega_{méc} = \Omega_t.G \; ; \; C_t = C_g.G \tag{6}$$

The fundamental equation of dynamics can be written:

$$C_{méc} = J\frac{d\Omega_{méc}}{dt} = C_g - C_{em} - f.\Omega_{méc} \tag{7}$$

2.2. Modelling of DFIG

The modelling of the DFIG is similar to the induction generator, the only difference is that the rotor windings are not short-circuited. The DFIG is represented in the park frame by the following equations [3, 15]:

$$\begin{cases} v_{sd} = -R_s i_{sd} + \frac{d\phi_{sd}}{dt} - w_s\phi_{sq} \\ v_{sq} = -R_s i_{sq} + \frac{d\phi_{sq}}{dt} + w_s\phi_{sd} \\ v_{rd} = -R_r i_{rd} + \frac{d\phi_{rd}}{dt} - w_s\phi_{rq} \\ v_{rq} = -R_r i_{rq} + \frac{d\phi_{rq}}{dt} + w_s\phi_{rd} \end{cases} \tag{8}$$

$$\begin{cases} \phi_{sd} = -L_s i_{sd} - M i_{rd} \\ \phi_{sq} = -L_s i_{sq} - M i_{rq} \\ \phi_{rd} = -L_s i_{rd} - M i_{sd} \\ \phi_{rd} = -L_s i_{rq} - M i_{sq} \end{cases} \tag{9}$$

V being the voltage (V), i is the current (A), ω_s and ω_r are angular speed of the rotating field referred respectively to the stator and the rotor (rad/s), Rs and Rr are respectively stator and rotor resistance (Ω), Φsand Φr are the stator and the rotor flux. The electromagnetic torque can be expressed as a function of the stator flux and current:

$$C_{em} = p\frac{M}{L_s}(\phi_{sq}i_{rd} - \phi_{sd}i_{rq}) \tag{10}$$

The stator active and reactive power are given by the following expression:

$$\begin{cases} P_s = Re\{v_s i_s^*\} = (v_{sd} i_{sd} + v_{sq} i_{sq}) \\ Q_s = Im\{v_s i_s^*\} = (v_{sq} i_{sd} - v_{sd} i_{sq}) \end{cases} \quad (11)$$

3. Control Strategies of DFIG

Fig.3 shows that in order to ensure the highest energy conversion efficiency the DFIG must operates at a variable speed following the optimum power characteristics $P_{max}=f(\Omega_{opt})$ (with Ω_{opt} corresponding to C_{pmax}). Therefore, at a given wind speed, the turbine must have been exposed to a resistive mechanical torque $C_{em\text{-}ref}$, or in other words an active power $P_{s\text{-}ref}$ delivered by the DFIG.

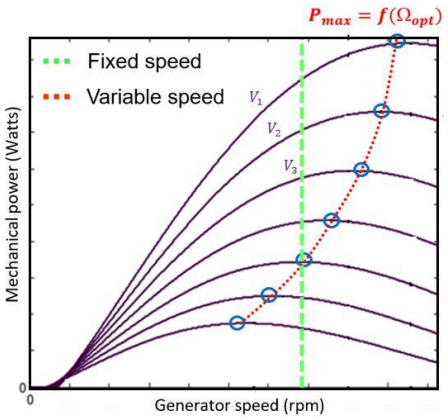

Fig. 3: Optimum power characteristic of the wind turbine

3.1. *Reference choice for the two-phase DFIG model*

In order to achieve independent control of active and reactive power, a two-phase *d-q* rotating reference frame is chosen related to the stator field **Fig.4** [3, 15]. Such as:

$$\Phi_{sd} = \Phi_s \quad \& \quad \Phi_{sq} = 0 \quad (12)$$

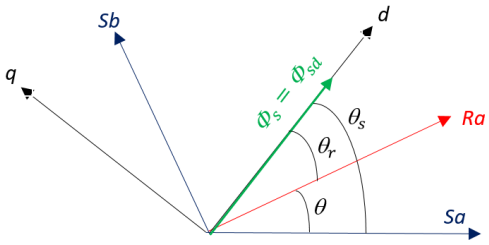

Fig. 4 : Orientation of Stator flux on d axis

The electromagnetic torque equation is then:

$$C_{em} = -p\frac{M}{L_s}\phi_{sd} i_{rq} \quad (13)$$

The equations of the stator flux can be rewritten as follows:

$$\begin{cases} \phi_s = -L_s i_{sd} - M i_{rd} \\ 0 = -L_s i_{sq} - M i_{rq} \end{cases} \quad (14)$$

For medium and high power generators used in wind turbine, the stator resistance Rs can be neglected [5, 10, 14]. In addition, assuming a stable grid which provides a constant stator flux Φs, allows us to simplify the stator voltages expressions, thus:

$$\begin{cases} v_{sd} = \frac{d\phi_s}{dt} = 0 \\ v_{sq} = w_s \phi_s = v_s \end{cases} \quad (15)$$

The stator currents can be expressed in terms of rotor currents as follows:

$$\begin{cases} i_{sd} = -\frac{\phi_s}{L_s} - \frac{M}{L_s} i_{rd} \\ i_{sq} = -\frac{M}{L_s} i_{rq} \end{cases} \quad (16)$$

Replacing stator currents expression in (9), rotor flux expressions can be rewritten as:

$$\begin{cases} \phi_{rd} = -\left(L_r - \frac{M^2}{L_s}\right) i_{rd} + \frac{M v_s}{w_s L_s} \\ \phi_{rq} = -\left(L_r - \frac{M^2}{L_s}\right) i_{rq} \end{cases} \quad (17)$$

The expressions of rotor flux equation (19) is integrated to (9). As a result, we can establish the relations between rotor currents and voltages we obtain:

$$\begin{cases} v_{rd} = -R_r i_{rd} - \left(L_r - \frac{M^2}{L_s}\right)\frac{di_{rd}}{dt} - gw_s\left(L_r - \frac{M^2}{L_s}\right) i_{rq} \\ v_{rq} = -R_r i_{rq} - \left(L_r - \frac{M^2}{L_s}\right)\frac{di_{rq}}{dt} - gw_s\left(L_r - \frac{M^2}{L_s}\right) i_{rd} + gw_s \frac{M}{L_s}\phi_s \end{cases} \quad (18)$$

$\sigma = 1 - \frac{M^2}{L_s L_r}$ Is constant called the dispersion coefficient.

$$\begin{cases} i_{rd} = \left(\frac{-1}{R_r + pL_r\sigma}\right)_s \left(V_{rd} - (gw_s L_r \sigma) i_{rq}\right) \\ v_{rq} = \left(\frac{-1}{R_r + pL_r\sigma}\right)_s \left(V_{rq} - (gw_s L_r \sigma) i_{rq} - gw_s \frac{M}{L_s}\phi_s\right) \end{cases} \quad (19)$$

Finally, according to (13), (17) and (18):

$$\begin{cases} P_s = -v_s \frac{M}{L_s} i_{rq} \\ Q_s = -v_s \frac{\phi_s}{L_s} - v_s \frac{M}{L_s} i_{rd} \end{cases} \quad (20)$$

From the above equations, we can develop a block diagram of the DFIG to regulate **Fig.5**, the DFIG model become approximately decomposed in two decoupled subsystems.

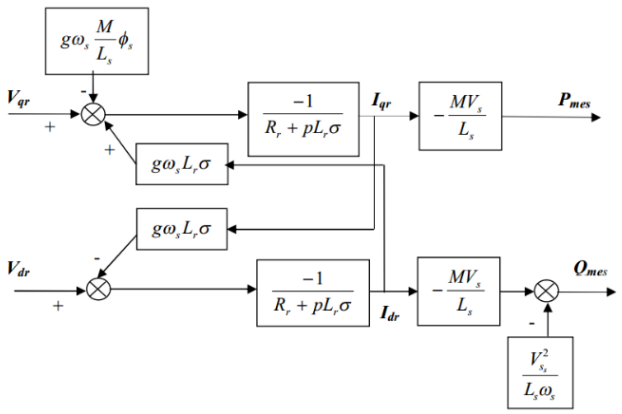

Fig. 5 : Block diagram of DFIG to regulate

3.2. *Proportional Integral (PI) controller design*

The PI controller is the most commonly used and the easiest to synthetize for DFIG control purposes, and in many industrial control schemes. This type of regulator is a combination of both proportional and integral action. It has the effect of improving simultaneously the steady and transient states.

Working Assumption [5]:

- According to the block diagram of DFIG **Fig.5**. Before proceeding with the regulator designs, a compensation block given by the following equations must be added after the PI controller:

$$\begin{cases} e_d = +g\dfrac{v_s M}{L_s} \\ e_q = \dfrac{v_s^2}{L_s w_s}\dfrac{L_s}{M v_s}\left(R_r + pL_r\sigma\right) \end{cases} \quad (21)$$

In steady state, we can write:

$$\begin{cases} e_d = +g\dfrac{v_s M}{L_s} \\ e_q = \dfrac{v_s^2}{L_s w_s}\dfrac{L_s}{M v_s} R_r \end{cases} \quad (22)$$

- The influence of coupling terms between the two axes **Fig. 5** is minimal which allows us to control each axis independently [9,8].
- The dynamic of the inverter is very quick compared the machine. In this case, the inverter model can be reduced to its static gain K=1 which reduces the system order.

A typical structure of a PI control system is shown in **Fig.6**. The error signal e(t) is used to generate the proportional and integral actions, with the resulting signals weighted and summed to form the control signal u(t) applied to the plant model.

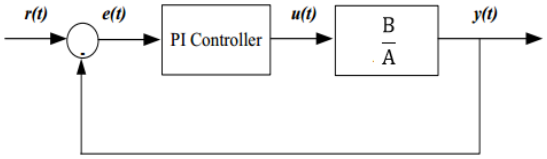

Fig. 6 : A typical PI controller structure

With: $A = L_s R_r + pL_s L_r\sigma \;;\; B = U_s M$

The open loop transfer function is given by:

$$G(p) = \left(k_p + \frac{k_i}{p}\right)\left(\frac{v_s M}{L_s R_r + pL_s L_r\sigma}\right) = \frac{\left(p + \dfrac{k_i}{k_p}\right)}{\left(\dfrac{p}{k_p}\right)}\frac{\dfrac{v_s M}{L_s L_r\sigma}}{\left(\dfrac{R_r}{L_r\sigma} + p\right)} \quad (24)$$

To eliminate the zero of the transfer function (the compensation method) we choose:

$$\frac{k_i}{k_p} = \frac{R_r}{L_r\sigma} \quad (25)$$

The open loop transfer function becomes:

$$G(p) = \frac{k_p\dfrac{v_s M}{L_s L_r\sigma}}{p} = \frac{1}{\tau_r p} \;;\; \tau_r = \frac{L_s L_r\sigma}{k_p v_s M} \quad (26)$$

The closed loop transfer function can be expressed as:

$$F(p) = \frac{1}{1+\tau_r p} \quad (27)$$

Finally, we get:

$$\begin{cases} k_p = \dfrac{1}{10.10^{-3}}\dfrac{L_s L_r\sigma}{v_s M} \\ k_i = \dfrac{1}{10.10^{-3}}\dfrac{L_s R_r}{v_s M} \end{cases} \quad (28)$$

In this study, the time constant is set to 10ms, which corresponds to a fast enough value for a medium and high power energy conversion system [5].

3.3. *Backstepping controller design*

The arrival of " Backstepping " provides a systematic technique to decompose a complex nonlinear control design problem into smaller and simpler subsystems, by the use of so-called “virtual control”. Backstepping technique was developed in the early 90 by Kanellakopoulos (1991) and inspired by the work of Feurer& Morse (1978) on one hand and Tsinias (1989) and Kokotović & Sussmann (1989) on the other. This method of control design is divided into various steps. In each step, we essentially deal with a simpler and easier single input single output design problem, and each step provides a reference for the next design step. The overall system’s stability and performance are achieved by a *Lyapunov* function.

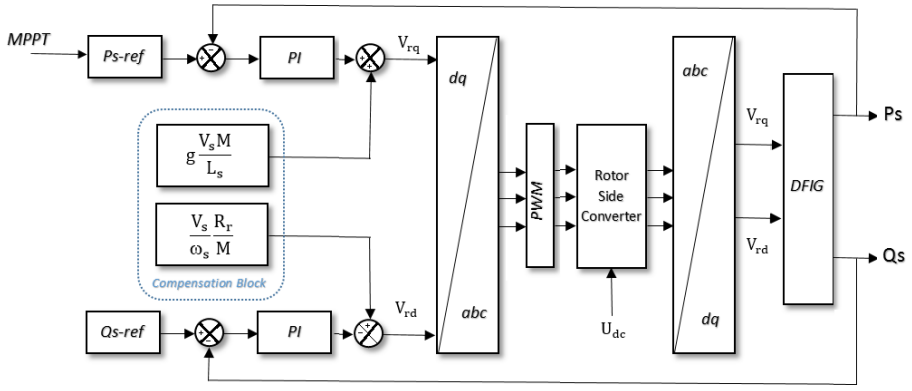

Fig. 7: Block Diagram of the proposed PI control design

In this section, we present a backstepping control approach applied to DFIG. The control scheme is designed in a way to keep the same general structure of the field oriented control. The synthesis of this control can be achieved in two steps. The DFIG model **Fig.5** can be presented as differential equations of active and reactive power, and rotor currents in the park frame, as follows:

$$\begin{cases} \dot{P}_s = -v_s \dfrac{M}{L_s \alpha}(V_{rq} + R_r I_{rq} + g\omega_s \alpha I_{rd} - g\dfrac{Mv_s}{L_s}) \\ \dot{I}_{rq} = -\dfrac{1}{\alpha}(V_{rq} + R_r I_{rq} + g\omega_s \alpha I_{rd} - g\dfrac{Mv_s}{L_s}) \\ y_1 = P_s \end{cases} \quad (29)$$

Moreover:

$$\begin{cases} \dot{Q}_s = -v_s \dfrac{M}{L_s \alpha}(V_{rd} + R_r I_{rd} - g\omega_s \alpha I_{rq}) \\ \dot{I}_{rd} = -\dfrac{1}{\alpha}(V_{rq} + R_r I_{rd} - g\omega_s \alpha I_{rq}) \\ y_2 = Q_s \end{cases} \quad (30)$$

With: $\alpha = L_r \sigma = (L_r - \dfrac{M^2}{L_s})$

➢ *Step 1: Computation of the currents reference*

We select the first two subsystems from (30) and (31). The output of the first subsystem P_s must tend to P_{s_ref} and the output of the second subsystem Q_s must tend to Q_{s_ref}. We define (e1, e3) representing the errors variables:

$$\begin{aligned} e_1 &= P_{s-ref} - P_s \quad \Rightarrow \dot{e}_1 = \dot{P}_{s-ref} - \dot{P}_s \\ e_3 &= Q_{s-ref} - Q_s \quad \Rightarrow \dot{e}_3 = \dot{Q}_{s-ref} - \dot{Q}_s \end{aligned} \quad (31)$$

Virtual control variables are I_{rd} and I_{rq}. The first *Lyapunov* functions are chosen such that:

$$V_1 = \frac{1}{2}e_1^2 \; ; \; V_3 = \frac{1}{2}e_3^2 \quad (32)$$

Using the equation (32):

$$\begin{cases} \dot{V}_1 = e_1 \dot{e}_1 = e_1 \left\{ \dot{P}_{s-ref} - \dfrac{v_s M}{L_s \alpha}\left(V_{rq} + R_r I_{rq} + g\omega_s \alpha I_{rd} - g\dfrac{Mv_s}{L_s} \right) \right\} \\ \dot{V}_3 = e_3 \dot{e}_3 = e_3 \left\{ \dot{Q}_{s-ref} - \dfrac{v_s M}{L_s \alpha}\left(V_{rd} + R_r I_{rd} - g\omega_s \alpha I_{rq} \right) \right\} \end{cases} \quad (33)$$

To guarantee a stable tracking the derivative of V_1 and V_2 must be negative (*Lyapunov* second theory). This allows the synthesis of rotor current references (virtual control variables), such as:

$$\begin{cases} \left\{ \dot{P}_{s-ref} - \dfrac{v_s M}{L_s \alpha}\left(V_{rq} + R_r I_{rq} + g\omega_s \alpha I_{rd} - g\dfrac{Mv_s}{L_s} \right) \right\} = -k_1 e_1 \\ \left\{ \dot{Q}_{s-ref} - \dfrac{v_s M}{L_s \alpha}\left(V_{rd} + R_r I_{rd} - g\omega_s \alpha I_{rq} \right) \right\} = -k_3 e_3 \end{cases} \quad (34)$$

This allows finding the desired current control state, either:

$$\begin{cases} I_{rq-ref} = \dfrac{L_s \alpha}{v_s M R_r}\left(\dot{P}_{s-ref} + k_1 e_1 \right) - \dfrac{1}{R_r}\left(V_{rq} + g\omega_s \alpha I_{rd} - g\dfrac{v_s M}{L_s} \right) \\ I_{rd-ref} = \dfrac{L_s \alpha}{v_s M R_r}\left(\dot{Q}_{s-ref} + k_3 e_3 \right) - \dfrac{1}{R_r}\left(V_{rd} - g\omega_s \alpha I_{rq} \right) \end{cases} \quad (35)$$

Therefore, the control variables are asymptotically stable.

➢ *Step 2: Computation of the control voltages*

The currents determined previously, are the desired variable for this step. We define the errors e2 and e4:

$$\begin{aligned} e_2 &= I_{rq-ref} - I_{rq} \quad \Rightarrow \dot{e}_2 = \dot{I}_{rq-ref} - \dot{I}_{rq} \\ e_4 &= I_{rd-ref} - I_{rd} \quad \Rightarrow \dot{e}_4 = \dot{I}_{rd-ref} - \dot{I}_{rd} \end{aligned} \quad (36)$$

V_{rq} and V_{rd} are now the real control signals. The new *Lyapunov* function are chosen as:

$$V_2 = \frac{1}{2}(e_1^2 + e_2^2) \; ; \; V_4 = \frac{1}{2}(e_3^2 + e_4^2) \quad (37)$$

Using the equation (36) the derivative of functions (37):

$$\begin{cases} \dot{V}_2 = e_1 \left\{ \dot{P}_{s-ref} - \dfrac{v_s M}{L_s \alpha}\left(V_{rq} + R_r (I_{rq-ref} - e_2) + g\omega_s \alpha I_{rd} - g\dfrac{Mv_s}{L_s} \right) \right\} \\ \quad + e_2 \left\{ \dot{I}_{rq-ref} + \dfrac{1}{\alpha}\left(V_{rq} + R_r (I_{rq-ref} - e_2) + g\omega_s \alpha I_{rd} - g\dfrac{Mv_s}{L_s} \right) \right\} \\ \dot{V}_4 = e_3 \left\{ \dot{Q}_{s-ref} - \dfrac{v_s M}{L_s \alpha}\left(V_{rd} + R_r (I_{rd-ref} - e_2) - g\omega_s \alpha I_{rq} \right) \right\} \\ \quad + e_4 \left\{ \dot{I}_{rd-ref} - \dfrac{v_s M}{L_s \alpha}\left(V_{rd} + R_r (I_{rd-ref} - e_2) - g\omega_s \alpha I_{rq} \right) \right\} \end{cases} \quad (38)$$

In order to guarantee a stable tracking the control voltages V_{rd} and V_{rq} are deduced as follow:

$$\begin{cases} V_{rq-C} = \left(-k_2 e_2 - \dot{I}_{rq-ref} - \dfrac{v_s M R_r}{L_s \alpha} e_1 \right) \alpha - \left(R_r I_{rq} + g\omega_s \alpha I_{rd} + g\dfrac{v_s M}{L_s} \right) \\ V_{rd-C} = \left(-k_4 e_4 - \dot{I}_{rd-ref} - \dfrac{v_s M R_r}{L_s \alpha} e_3 \right) \alpha - \left(R_r I_{rd} - g\omega_s \alpha I_{rd} \right) \end{cases} \quad (39)$$

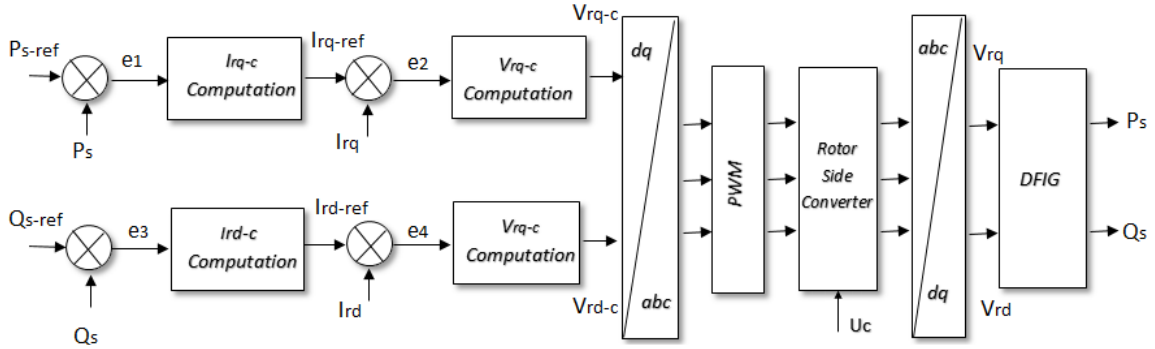

Fig. 8: Block Diagram of the proposed Backstepping approach control design

The derivative of equation is given by:

$$\dot{V}_2 = -k_1 e_1^2 - k_2 e_2^2 \langle 0 \;\; ; \;\; \dot{V}_4 = -k_3 e_3^2 - k_4 e_4^2 \langle 0$$

This allows concluding that the system is globally asymptotically stable.k_1, k_2, $k_3$and k_4 are positive constants, the good choice of these parameters guarantee the stability, and a fast dynamic response.

The block diagram of the proposed control scheme is illustrated in **Fig.8**. The PI controller is replaced by four blocks that represent the backstepping approach. The "$I_{rq\text{-}c}$ computation" and "$I_{rd\text{-}c}$ computation" blocks provides respectively the rotor currents references components $I_{rq\text{-}ref}$, $I_{rd\text{-}ref}$ (virtual control variables) via the active and the reactive power feedback controls From Eq. (35). Moreover, the voltages commands $V_{rq\text{-}c}$, $V_{rd\text{-}c}$ are generated by the "$V_{rq\text{-}c}$ Computation" and "$V_{rd\text{-}c}$ Computation" blocks via the rotor currents feedback control of according to (39).

3.4. *Maximum power point tracking:*

Wind energy, even though abundant, varies continuously due to the fluctuating nature of the wind speed. The power captured by the turbine depends mainly on the power coefficient Cp, which is a function of the speed of the generator (or TSR λ). Maintaining Cp at its maximum value allows the wind-energy conversion systems to produce all the power they are capable of.

Several maximum power extraction algorithms exist in the literature. This paper, focus on the TSR control, using a backstepping controller, we regulate the rotational speed of the DFIG, in order to maintain the TSR to its optimum value ($\lambda_{Cp\text{-}max}$) at which power extracted is maximum. This method requires the measurement or the estimation of both the wind speed and the turbine speed, and the turbine optimum TSR **Fig.2** (corresponding to C_{pmax}) must be known.

The angular rotation speed $\Omega_{t\text{-}opt}$ that corresponds to the optimum value of TSR (λ_{Cp-max}) is given by:

$$\Omega_{t-opt} = \frac{\lambda_{Cp-max}}{V_1} R \qquad (40)$$

And according to (6) we can write:

$$\Omega_{méc-ref} = \Omega_{t-opt}.G \qquad (41)$$

All recent models of digital MPPT controllers available are microprocessors controllers. In this work, we used a backstepping algorithm to develop the control law allowing the system to follow the desired trajectory. We have:

$$J\frac{d\Omega_{méc}}{dt} = C_g - C_{em} - f.\Omega_{méc} \qquad (42)$$

- *Step 1: Computation of the control variable*

We define e that represents the error variable:

$$e(\Omega) = \Omega_{ref} - \Omega \;\; \Rightarrow \dot{e}(\Omega) = \dot{\Omega}_{ref} - \dot{\Omega} \qquad (43)$$

We select the quadratic Lyapunov function:

$$V_1 = \frac{1}{2} e^2 \qquad (44)$$

The derivative of (44) is given by:

$$\dot{V}_1 = e(\Omega)\dot{e}(\Omega) = e(\Omega)\left(\dot{\Omega}_{ref} - \dot{\Omega}\right) \qquad (45)$$

By setting (42) in (45) we obtain:

$$\dot{V}_1 = e(\Omega)\left(\dot{\Omega}_{ref} - \frac{1}{J}\left(C_g - C_{em} - f.\Omega_{méc}\right)\right) \qquad (46)$$

In order to guarantee a stable tracking C_{em} is chosen such that:

$$\left(\dot{\Omega}_{ref} - \frac{1}{J}\left(C_g - C_{em} - f.\Omega_{méc}\right)\right) = -ke \qquad (47)$$

k is a positive constant, finaly we get :

$$C_{em} = J\left(\dot{\Omega}_{ref} + ke(\Omega)\right) + C_g + f.\Omega_{méc} \qquad (48)$$

We have $\dot{V}_1 = -ke^2 \langle 0$. Therefore, according to Lyapunov the system is globally asymptotically stable.

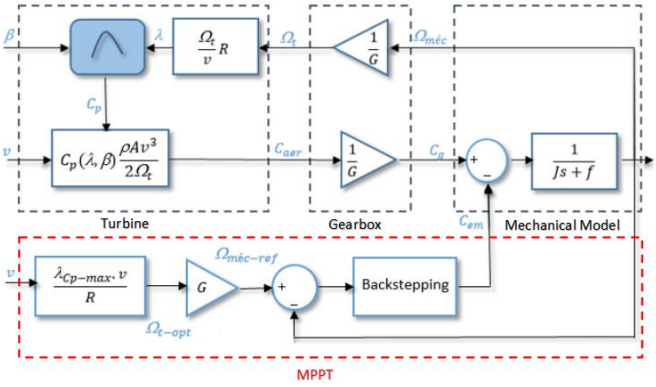

Fig. 9: Maximum power point tracking using backstepping

4. Simulations Results

In this section, we will test and compare the performance of the different controllers presented in the previous section. We have made three simulations for each, to conclude on the convergence properties and stability of the overall closed loop system, disturbance rejection and robustness.

The proposed DFIG control has been simulated using Matlab/Simulink. DFIG parameters are those in appendix. In order to satisfy the convergence and stability conditions, the adjustment parameters of our backstepping approach are chosen as follows: k1= 80000, k2=5000, k3=90000 and k4=6000 to satisfy convergence condition.

4.1. *Dynamic performances*

The modelling of the wind profile requires climatic and geographical data of the concerned site, as well as the period of the year concerned by the study. Therefore, several researches have been carried out. In this work, the wind profile is modelled in deterministic form by a sum of several harmonics, around an average speed **Fig.10**:

$$V(t) = A + \sum_{k=1}^{i} a_k . \sin\left(b_k w_v t\right) \qquad (49)$$

Where A is the mean value of wind speed, a_k and $b_k.w_v$ are respectively the amplitude and the pulsation of the harmonic of order k.

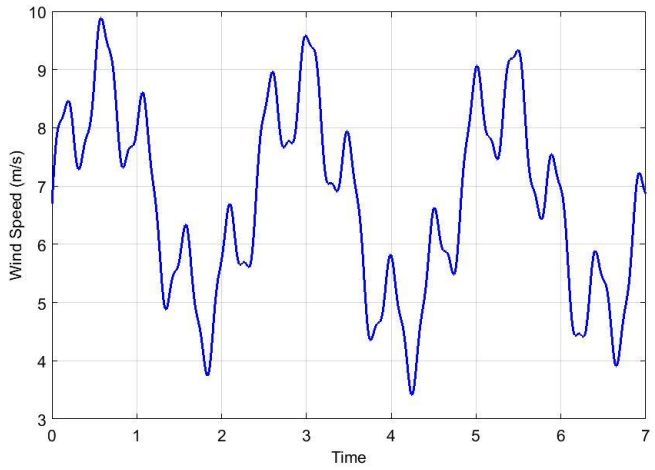

Fig. 10: Wind speed (m/s)

The wind conversion system model includes: wind turbine, Double-fed induction generator (DFIG), two power converters (the rotor side converter and the grid side converter) controlled by the space vector PWM, used to connect the rotor of DFIG to the grid **Fig.1**.

The blades orientation angle is fixed β=2°, a characteristics resulting from a real measurements on a real wind turbines show the this value is valid for power variation ranging from 0 to approximately 1.5Mw (rated power) **[14]**. Beyond this limit, this angle must be controlled in order to maintain the power generated by the DFIG constant.

The maximum power point tracking "MPPT" technique described in section 3, has as shown in **Fig.11** kept the power coefficient Cp at its maximum value which corresponds for β=2° to $C_{p\text{-}max}$=0.437.

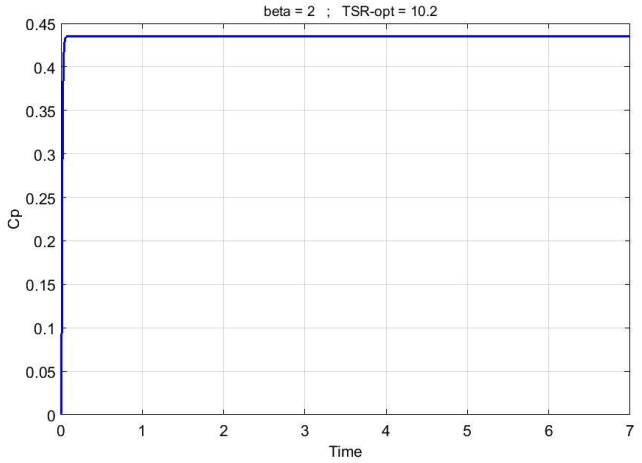

Fig. 11: Power coefficient β=2° Cp-max=0.44; λopt= 10.2

The active power Ps-ref is a function of the wind speed, based on the open loop MPPT test. The reactive power Qs-ref is maintained at zero to keep a unitary power factor [8]. Simulation results of the overall model of wind-energy conversion system are presented in **Fig.12** and **Fig.3**. By these figures, we illustrate the active and reactive power variations.

In brief, for the first simulation, we can observe that with both backstepping and PI controller, the output of our systems converges perfectly to their reference values of the active and reactive power (Ps-ref, Qs-ref) coming from the control in MPPT operation conditions of the wind turbine, all tracking errors converge to zero asymptotically. The wind captured active power has the same shape as the wind profile applied (it is considered negative because it is a generated power) However, the obtained results shows the superiority of the backstepping approach in terms of the response time (T_{PI}=0.8sec, T_{BS}=0.005sec). On the other hand, in the context of this test, the performance of these regulators can be considered equivalent.

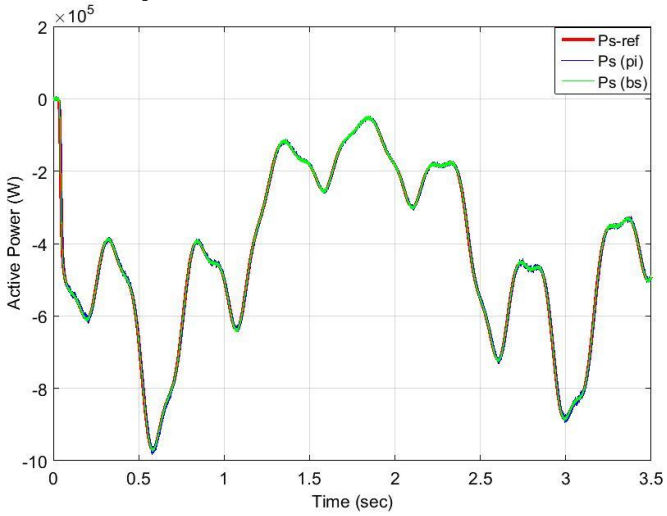

Fig. 12 : Active Power

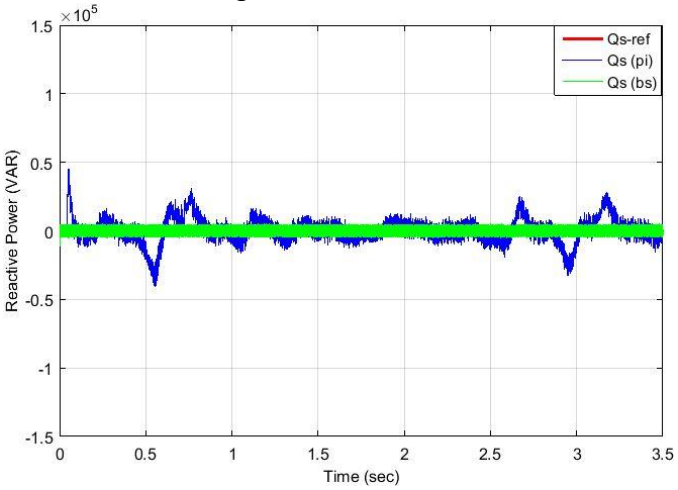

Fig. 13: Reactive Power

4.2. *Disturbance rejection*

A good disturbance rejection is characterized by a quick return of the error to zero. Therefore, in this case, we use a high fluctuations wind speed profile to observe the capability of our controllers to act against this kind of disturbance.

The differences between PI regulator and the proposed backstepping approach appears clearly in this simulation **Fig.14** and **Fig.15**. Unlike the backstepping the PI regulators are very sensitive to the perturbation that we creates, we can remark a significant deviation from the reference values especially in reactive power control figure **Fig.15**. Now that,

the synthesis of this type of controllers is based on transfer functions without expecting any disturbance. On the other hand, backstepping controller shows excellent rejection of disturbance and a satisfactory tracking performance respectively of active and reactive power.

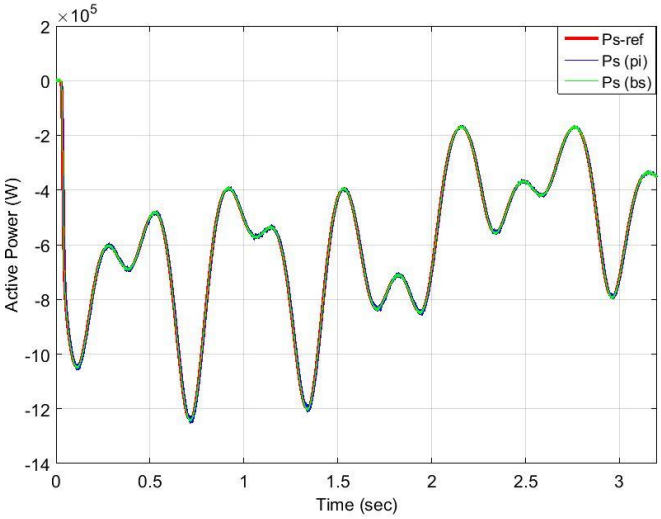

Fig. 14: Active Power

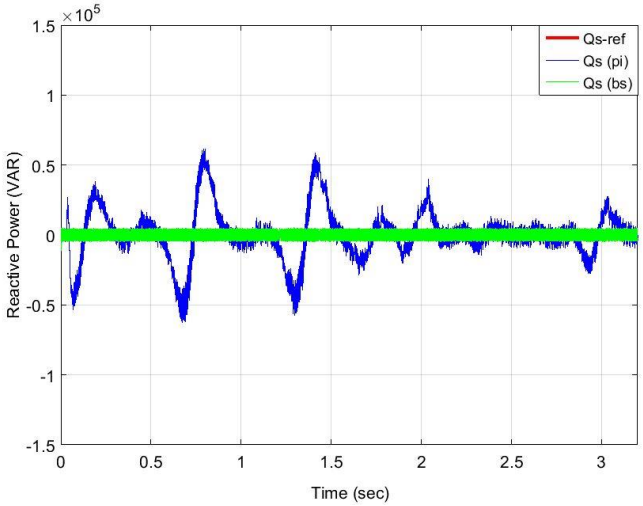

Fig. 15: Reactive Power

4.3. *Robustness*

In the previous tests, both PI and backstepping regulators were synthesized assuming that the machine parameters are fixed. In fact, several physical phenomena cause variations of these parameters e.g. (a rise in temperature increases the resistance values, inductors saturation…). Moreover, the identification of these parameters is exposed to inaccuracies due to the methodology adopted and the measuring devices. Hence, it is particularly interesting to compare both systems performances against such a phenomena.

To demonstrate the performance of each regulator against the model uncertainties that affect stability of the closed-loop systems. This test consists of varying the model parameters used in the DFIG:

$$Rr' = 2Rr \; ; \; Ls' = 1.2Ls \; ; \; Lr' = 1.2Lr;$$

Fig. 16 and **Fig.17** shows that the influence of parameter variations is higher with the PI controller than with backstepping controller. The response time of the PI controller has been significantly increased. Whereas the backstepping control scheme provide a good behaviour in the case of a large parametric variation.

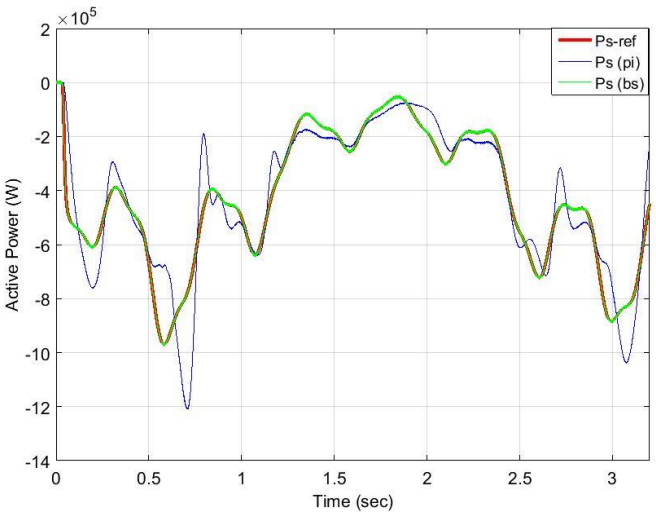

Fig. 16: Active Power

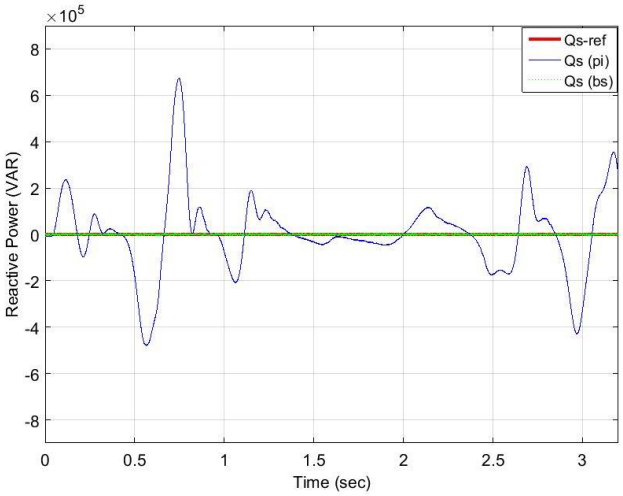

Fig. 17: Reactive Power

5. Conclusion

This work has been devoted to the modelling and control design of DFIG integrated into a wind energy conversion system operating at variable speed. In the first phase, we present the modelling of the wind turbine and the DFIG based on physical equations. Next, we introduced the field oriented control scheme of DFIG, in order to ensure a flexible and independent control of its active and reactive power exchanged (collected and injected) between the stator and the grid. Then, a MPPT technique is presented using a backstepping algorithm to control the mechanical speed, so that the power coefficient Cp can be kept at its maximum value. Thus, the maximum wind power is extracted. In the second phase, we have designed and compared two control strategies applied to DFIG. First, a PI regulator is developed. Secondly, a backstepping control scheme is proposed.

The open loop MPPT block diagram provide the active power reference for our control schemes, while the reactive power is maintained equal to zero, so that we keep a unitary power factor for the grid [8]. The simulation results allows us to show the proposed algorithms capabilities to react, in terms of tracking performances, disturbance rejection, and robustness against parametric variations. We have made three simulations for each control scheme. All in all, from a conceptual point of view, we noticed that the proposed backstepping approach provides more meaningful results compared to the PI control. Therefore, this strategy is offers a good candidate for controlling DFIG integrated into a wind energy conversion system interconnected to the grid.

Appendix

TABLE 1

Wind Turbine data	
Blade radius	*R=35*
Power Coefficient	*Cp max=0.44*
Optimal relative wind speed	*λ max=10.2*
Mechanical speed multiplier	*G=60*
Moment of inertia	*J=0.41*
Damping coefficient	*F=0.017*
Density of air	*d=1.2*

TABLE 2

Double Fed Induction Generator data	
Rated Power	1.5MW
Rated stator voltage	vs=690V
Nominal frequency	fs=50Hz
Number of pole pair	P=2
Rotor Resistance	Rr=0.021
Stator Resistance	Rs=0.012
Rotor Inductance	Lr=0.01367
Stator Inductance	Ls=0.0137
Mutual Inductance	M=0.0135

References

[1] B. Bousoufi, M. Karim, A. Lagrioui, M. Taoussi, A. Derouich, “Adaptive Backstepping Control of DFIG Generators for Variable-speed Wind Turbines system”. International Journal of Computers and Technology, IJCT. Vol.12, No.7. 2014. (Article)

[2] N. Khemiri, A. Khedher, M. Faouzi. “Wind Energy Conversion System using DFIG Controlled by Backstepping and Sliding Mode Strategies”. International Journal of Renewable Energy Research, IJRER. Nihel Khemiri et al., Vol.2, No.3, 2012. (Article)

[3] Intissar Moussa, Adel Bouallegue, Adel Khedher. “3kW Wind Turbine Emulator Implementation on FPGA Using Matlab/Simulink”. International Journal of Renewable Energy Research, IJRER. I. Moussa et al., Vol.5, No.4, 2015. (Article)

[4] Hassan Mahmoudi, Madiha El Ghamrasni, Ahmed Largrioui, Badre Bossoufi. “Backstepping Adaptive Control of DFIG Generators for Wind Turbines Variable-Speed” Journal of Theoretical and Applied Information Technology. Vol.81, No.2 2015. (Article)

[5] F. Poitiers, T. Bouaouiche, M. Machmoum., “Advanced control of a doubly-fed induction generator for wind energy conversion”, Electric Power Systems Research, Vol.79, pp.1085–1096, 2009. (Conference paper)

[6] Iman. Nouira, Adel Khedher. “A Contribution to the Design and the Installation of a Universal Platform of a Wind Emulator using a DC Motor”. International Journal of Renewable Energy Research, IJRER. Imen Nouira et al., Vol.2, No.4, 2012 (Article)

[7] J. Ben Alaya, A. Khedher and MF. Mimouni, “DTC and Nonlinear Vector Control Strategies Applied to the DFIG operated at Variable Speed”, WSEAS Transactions on environment and development, Vol. 6, No. 11, pp. 744-753, November 2010 (Article)

[8] E. Mahersi, A. Khedher, MF. Mimouni, “The Wind energy Conversion System Using PMSG Controlled by Vector Control and SMC Strategies”, International Journal of Renewable Energy Research, IJRER, Vol. 2, No.4, pp. 732-741, April 2012. (Article)

[9] BEKAKRA, Youcef & ATTOUS, D. Ben. “Sliding mode controls of active and reactive power of a DFIG with MPPT for variable speed wind energy conversion”. Australian Journal of Basic and Applied Sciences, 2011, vol. 5, no 12, p. 2274-2286. (Article)

[10] Khriss, Ali, Nasser, Tamou, et Essadki, Ahmed. “A Linear Active Disturbance Rejection Control applied for DFIG based Wind Energy Conversion System”. International Journal of Computer Science Issues (IJCSI), 2013, vol. 10, no 2, p. 391-399. (Article)

[11] Chakib, R., Essadki, A., & Cherkaoui, M. “Active Disturbance Rejection Control for Wind System Based on a DFIG”. World Academy of Science, Engineering and Technology, International Journal of Electrical, Computer, Energetic, Electronic and Communication Engineering, 2014, vol. 8, no 8, p. 1306-1315. (Article)

[12] F. Kendouli, K. Nabti, K. Abed, H. Benalla. "Modélisation, simulation et contrôle d’une turbine éolienne à vitesse variable basée sur la génératrice asynchrone à double alimentation". Revue des Energies Renouvelables, Vol.14, No.1, 2011. (Article)

[13] S.E. Ben Elghali. “Modélisation et Commande d’une Hydrolienne Equipée d’une Génératrice Asynchrone Double Alimentation”. European Journal of Elecrical Engineering. 2008. (Standards and Reports)

[14] Salma El AIMANI. “Modelisation de Differentes Technologies D’Eolienne Intégrées Dans un Réseau Moyenne Tension”. 2004. (Standards and Reports)

[15] Yousfi MESSAOUD, Synthese des Controlleurs par Backstepping de la Machine Asynchrone 2014. (Standards and Reports).

[16] Handan Nak, Ali Fuat Ergenc “A New Controller for Variable Speed Wind Turbine Generator”. International

Conference on Renewable Energy Research and Applications, ICRERA, 2013. (Conference paper).

[17] Abdel Ghani Aissaoui, Ahmed Tahour, Mohamed Abid, Najib Essounbouli, Frederic Nollet " Using Neuro Fuzzy PI Techniques in Wind Turbine Control" International Conference on Renewable Energy Research and Applications, ICRERA, 2013. (Conference paper).

[18] M.B.C Salles, A.J.S Filho and A.P.Grilo "A Study on the Rotor Side Control of DFIG-based Wind turbine during Voltage Sags without Crowbar System" International Conference on Renewable Energy Research and Applications, ICRERA, 2013. (Conference paper).

[19] Adinda Ihsani Putri, Minho Ahn, Jaeho Choi "Speed Sensorless Fuzzy MPPT Control of Grid Connected PMSG for Wind Power Generation" International Conference on Renewable Energy Research and Applications, ICRERA, 2012. (Conference paper).

[20] E.Aydin, A. Polat, L.T.E Ergene "Vector Control Of DFIG n Wind Power Application" International Conference on Renewable Energy Research and Applications, ICRERA, 2016. (Conference paper)